



Photocatalytic degradation of a trichromatic direct dye under direct solar irradiation: reaction pathway and identification of intermediate products

Meriem Kouhail^{a,b,*}, Zakia El Ahmadi^a, Abbés Benayada^a, Said Gmouh^c

^aLaboratory of Applied Geophysics, Geotechnics, Engineering Geology and the Environment, Mohammed-V University Rabat, Avenue Ibn Sina B.P 765, 10090 Rabat, Morocco, email: kouhail@esith.ac.ma/mkouhail@gmail.com

^bLEC – ESITH, Laboratory of Expertise and Control – Higher School of Textile and Clothing Industries, Km 8 route d’El Jadida B.P. 7731, Casablanca, Morocco, emails: Elahmadiz@gmail.com (Z. El Ahmadi), Benayada55@gmail.com (A. Benayada)

^cLaboratory of Engineering and Materials LIMAT, University Hassan II de Casablanca, Ben M’Sick Av Driss El Harti Sidi Othmane B.P 7955, Casablanca, Morocco, email: Said.gmouh@gmail.com (S. Gmouh)

Received 9 April 2020; Accepted 20 November 2020

ABSTRACT

ZnO was synthesized, characterized by scanning electron microscopy, X-ray diffraction, UV-visible spectrophotometry, and infrared spectroscopy analysis, and then it was applied as a photocatalyst for trichromatic direct dye: Direct Yellow 86 (DY86), Direct Red (DR243), and Direct Blue (DB71) under solar irradiation. The progress of photocatalytic degradation was observed by monitoring the change in substrate concentration, employing UV-visible spectrophotometer and high-performance liquid chromatography. The order of degradation was $DB71 \geq DR243 > DY86$. A detailed study was also carried out using liquid chromatography/tandem mass spectrometry to determine the degradation pathway of the dye, as well as to confirm the order of degradation and to identify some of the intermediate products formed; a possible degradation mechanism was also proposed. The effects of parameters such as time, pH, and salt were studied, and the mineralization was confirmed by chemical oxygen demand measurement. The synthesized ZnO nanoparticles could be reused, and the water obtained after treatment might be reused for a second dyeing process.

Keywords: Textile dye; Photocatalytic activity; Reusable water; LC/MS/MS; Solar irradiation

1. Introduction

The sustainable development of industry and society is becoming an overwhelming problem all over the world, it is responsible for the environment’s contamination caused by organic pollutants [1]. Among all the industrial sectors, the textile industry has traditionally been one of the most important industries, which releases a huge quantity of wastewater effluents during handling, particularly in the

washing and coloring steps with a variety of dyes [2,3]. Dyes can be classified in various classes, including acridine dyes, quinine–amine dyes, arylmethane dyes, anthraquinone dyes, nitro dyes, xanthenes dyes, and azo dyes [4,5].

The azo dyes and their degradation products are very toxic, carcinogenic, and can cause significant environmental pollution problems [3,6]; therefore, it is very important to treat azo dye wastewater before its discharge into the environment in order to reduce the impact of colored

* Corresponding author.

effluents into the ecosystem, and to enforce the effluent color standard which must become a serious concern for legislators in all countries [3]. Most of the processes such as physical, biological, electrochemical, and chemical have been either ineffective in treating these toxic effluents, and/or merely resulting in the transfer of toxicity from effluent to a huge amount of solid waste, except advanced oxidation photocatalytic (AOP) [6]. AOP has numerous advantages like (i) a wide application range, especially to the complex molecule–structure contaminants, which cannot be degraded by conventional methods; (ii) the selected catalysts present no toxicity to the human health, and (iii) a destructive power to pollutants, which can lead to total mineralization into CO_2 and H_2O [7]. But if the photocatalytic activity is not attained, intermediate dye products are formed; these intermediate products may be more toxic than the parent compound. Therefore, it is necessary to identify the degradation products [8]. Numerous analytical techniques, for example, the spectrophotometric methods like UV-VIS, diffuse reflectance (Fourier transform infrared (FTIR)), high-performance liquid chromatography (HPLC), and gas chromatography-mass spectrometry (GC-MS), were used for the determination of organic intermediate products, but all these methods cannot identify efficiently the nature of the intermediate product, because they cannot analyze the short-lifetime species produced during the reaction [9].

Sulfonated azo dyes and sulfonated molecules are non-volatile and highly soluble in water, therefore they cannot be analyzed by GC/MS. Moreover, hydrophilic reaction intermediates which still contain the chromophoric groups, cannot be extracted efficiently in the solvents usually used in GC-MS analysis [10]; consequently, these methods are inappropriate for intermediate products' identification. However, liquid chromatography/tandem mass spectrometry (LC/MS/MS) is the most appropriate technique; it has been employed in many cases such as separation, identification, and characterization of the photocatalytic degradation products [11]. This technique is also more recommended and applied to the detection of sulfonated, azoique, anthraquinone, and triphenylmethane dyes in the environment [12].

The photocatalytic degradation of dyes has been intensified throughout the world [13], however, only a few studies have made a comparison of decolorization and degradation between three dyes, with a synthesized photocatalyst. For this reason, the main objective of the present work is to investigate the degradation behaviors of trichromatic direct azo dye: Direct Yellow 86 (DY86), Direct Red (DR243), and Direct Blue (DB71) which are widely used to dye cotton and other cellulosic fibers with a synthesis zinc oxide (ZnO), after their characterization by scanning electron microscopy (SEM), X-ray diffraction (XRD), UV-visible spectrophotometry (UV-vis), and infrared spectroscopy (IR) analysis. The influence of contact time, pH, the presence of salts (NaCl), and the chemical structure of the dye is studied. The decolorization monitoring was followed by UV-vis, the degradation monitoring was carried out by HPLC-DAD, and the degradation pathway, possible intermediate products, and degradation mechanism were proposed by employing LC/MS/MS. The mineralization

was verified by chemical oxygen demand (COD) measurement. The reusability of ZnO and water obtained after photocatalytic treatment has also been studied.

2. Materials and methods

2.1. Chemicals

Zinc chloride (ZnCl_2) is a precursor for zinc oxide (ZnO) synthesis, ethanol, sodium hydroxide NaOH, and hydrochloric acid HCl; all the used reagents were of analytical grade and were purchased from Sigma Aldrich, and no further purification was done before using them.

2.2. Pollutants

Direct dyes were chosen as an exemplary pollutant to evaluate the photocatalysis capabilities of this material. The chemical structure and a molecular formula of the direct dyes (Direct Yellow 86: DY86: $\text{C}_{39}\text{H}_{30}\text{N}_2\text{Na}_4\text{O}_{13}\text{S}_4$ /Direct Red 243: DR243: $\text{C}_{38}\text{H}_{28}\text{N}_2\text{Na}_4\text{O}_{17}\text{S}_4$ /Direct Blue 71: $\text{C}_{40}\text{H}_{23}\text{N}_7\text{Na}_4\text{O}_{13}\text{S}_4$: DB71) are shown in Table 1.

2.3. Preparation of the photocatalyst

2.3.1. ZnO

Zinc Oxide (ZnO) was prepared by the precipitation method; in a typical procedure, 1 mol of sodium hydroxide (NaOH) was dissolved in distilled water, this solution was heated at 90°C and after that, a solution of ZnCl_2 (0.5 M) was dropped for 30 min at 90°C . The drops of ZnCl_2 in the aqueous alkaline solution cause the immediate precipitation of ZnO, and the suspension color changes from transparent to white, this solution was stirred at 90°C for 2 h. The suspension was filtered, rinsed with distilled water three times, and then heated at 70°C for 4 h and calcined at 450°C for 2 h [14].

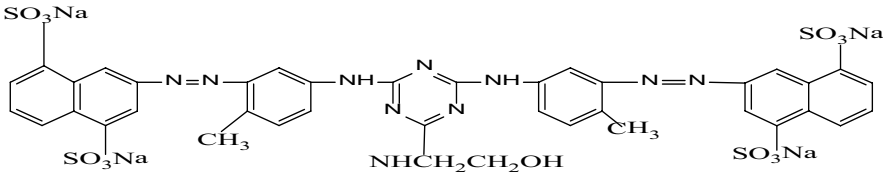
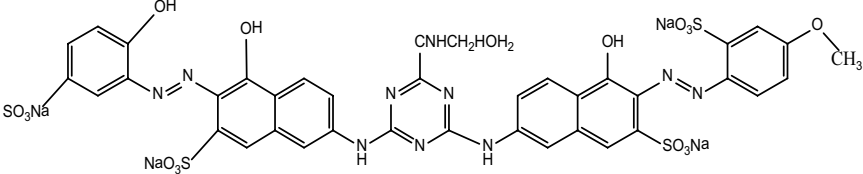
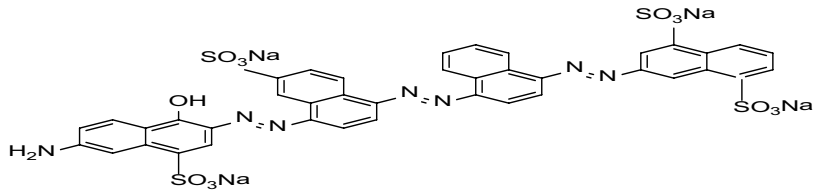
2.4. Characterizations of nanoparticles

The prepared nanoparticles were characterized on a PANalytical X'Pert diffractometer, with Cu ($K\alpha$) radiation ($\lambda = 1.5406 \text{ \AA}$) between 10° and 80° . The surface morphology was carried out by using an EROC HIROX CH 4000M SEM, and the FTIR was recorded on VETEX70; the precursor's spectrum was between 400 and $4,000 \text{ cm}^{-1}$. The optical properties of the catalyst were analyzed by diffuse reflectance UV-vis spectroscopy using a Shimadzu UV-vis spectrophotometer, with an integrating sphere and a spectral reflectance standard over a wavelength range of 200–800 nm.

2.5. Procedure experiment

Before conducting the experiments, an initial stock solution of each dye was prepared at a concentration of $1,000 \text{ mg L}^{-1}$, by dissolving a quantity of the dye in demineralized water. The trichromatic direct dyes were carried out in a batch system, containing 50 mL of dye solution with an unaltered pH_t , which was 7.0 for DY86, 7.6 for DR243, and 7.61 for DB71, with a unique concentration of (50 ppm), and the presence of (0.6 g L^{-1}) ZnO. The period

Table 1
Chemical structure of DY86, DR243, and DB71

Dye	Molecular structure
Direct Yellow 86 $\lambda = 403$	
Direct Red 243 $\lambda = 524$	
Direct Blue 71 $\lambda = 563$	

of solar light was 4 h, between 10 and 14 h under thermal agitation. The average intensity of sunlight during this period is 80,000 Lux units, measured with a lux meter Testo 545; every experiment is recorded in the same conditions (contact time, pH, anions, and irradiations' intensity). Various tests were carried out to evaluate the influence of the following process parameters: contact time, pH, and salt on the dye's photocatalysis. The first 30 min of the experiments are carried out in the dark to ensure the dyes' adsorption. All experiments were repeated three times, and average values were reported.

2.6. Chemical analyses

2.6.1. UV-vis spectrophotometer studies

The progress of the direct dye's photocatalytic decolorization was monitored by withdrawing a definite quantity of aliquot (2 mL) at regular intervals, and measuring the absorbance in UV-vis (Jasco V 730 spectrophotometer) for decolorization.

2.6.2. HPLC studies

The progress of photocatalytic degradation was measured using HPLC (Jasco type HPLC) which is composed of an SPG mode-graded pump, and a DAD® 2018 PLUS UV detector. The set is computer-controlled using the software: CHROMA NAV, version 2. The column is of type 5 DIPHENYL, and the lamps are of type D2 + WI. The eluting solvents are methanol (solvent A) and water quality (solvent B), with the proportions 80 (A)/20 (B). The flow rate of the mobile phase is set at 0.8 mL min⁻¹, and the injected volume is 15 µL for all the tests.

2.6.3. LC/MS/MS studies

The degradation products' identification was carried out on a LC/MS/MS (PerkinElmer ABSCIEX: 3200 Q TRAP), the product intermediates were separated using Phenomenex column (50 mm × 2 mm length), the mobile phase consisted of two solutions: acetonitrile and ammonium acetate with a gradient elution which was: 70/30, v/v, respectively, the flow rate of eluting was 0.08 mL min⁻¹, and the injection volume was 2 µL. The MS analysis was in the positive ions mode, and the mass range was 50–600 and 600–1,200 m/z.

2.7. Data treatment

The degradation and decolorization were controlled by taking a quantity of 2 mL of each solution at 30, 60, 120, 180, and 240 min, and measuring the residual concentration of each sample with the following Eq. (1):

$$C_r = \frac{C_t}{C_i} \quad (1)$$

where C_r is the residual concentration; C_t is the pollutant concentration at time t (mg L⁻¹), and C_i is the initial pollutant concentration (mg L⁻¹).

The kinetics study of DY86, DR243, and DB71 at 30 min, 60, 120, 180, and 240 dyes were carried out using zero-order, first-order, second-order, and Behnajady–Modirshahla–Ghanbery (BMG) reaction kinetics [15,16]:

Zero-order reaction kinetics is defined as in Eq. (2):

$$\frac{dC_t}{dt} = -k_0 \quad (2)$$

First-order reaction kinetics is denoted as in Eq. (3):

$$\frac{dC_t}{dt} = -k_1 C_t \tag{3}$$

Second-order reaction kinetics is expressed as in Eq. (4):

$$\frac{dC_t}{dt} = -k_2 (C_t)^2 \tag{4}$$

where k_0 , k_1 , and k_2 are the apparent kinetic rate constants of zero-, first-, and second-order kinetics, respectively, t is the reaction time, and C_t is the dye concentration at a given time t . By integrating Eqs. (2)–(4), the following equations could be achieved:

$$C_t = C_0 - k_0 t \tag{5}$$

$$C_t = C_0 e^{-k_1 t} \tag{6}$$

$$\frac{1}{C_t} = \frac{1}{C_0} + k_2 t \tag{7}$$

Eq. (7) is written in a linearized form as Eq. (8) [16]:

$$\ln C_t = \ln C_0 - k_1 t \tag{8}$$

BMG reaction kinetics is defined as in Eqs. (9) and (10) [20] below:

$$\frac{C_t}{C_0} = 1 - \left[\frac{t}{(m + b \cdot t)} \right] \tag{9}$$

Eq. (9) is written in a linearized form as:

$$\frac{t}{1 - \left(\frac{C_t}{C_0} \right)} = m + b \cdot t \tag{10}$$

where m and b are two characteristic constants relating to oxidation capacities and reaction kinetics [15]. By plotting t vs.

$\frac{t}{1 - \left(\frac{C_t}{C_0} \right)}$, a straight line with an intercept of m and a slope of b was obtained.

2.7.1. COD analysis

Measuring COD using the ST-COD (small-scale sealed-tube) method, according to the standard method NPT ISO 15705, determine the mineralization; this occurs at different times. The data were obtained and analyzed using the R parameter, as the COD efficiency in ($R\%$):

$$R = \frac{[\text{COD}]_0 - [\text{COD}]_t}{[\text{COD}]_0} \times 100 \tag{11}$$

where $[\text{COD}]_0$ and $[\text{COD}]_t$ are the initial and at any irradiation time COD values, respectively.

2.8. Reuse of the photocatalyst

To determine the recyclability and stability of ZnO, after the first experiment with a new catalyst (cycle 1), the nanoparticles were decanted, washed, and centrifuged at 5,000 rpm for 5 min, then they were reused for the next experience (cycle 2), by a fresh solution at the same experimental conditions under solar light. We followed the same protocol for all the next experiments (cycle 3, etc.).

2.9. Water recycling

2.9.1. Comparative study

To evaluate the possibility of reusing the water resulting from the photocatalytic treatment, a comparative study was made by two dyeing processes. The first one using obtained water after complete color decolorization with photocatalytic treatment (TW), and the second with deionized water (DW). This comparative study was made by dyeing two cotton fabric samples (A) and (B); sample (A) was dyed with deionized water (DW), and sample (B) was dyed with water obtained after complete color decolorization with photocatalytic treatments (TW). The bath of dyeing was prepared with the same quantity of colorant and salt at the same conditions, following the dyeing method (Fig. 1) in AHIBA NUANCE (TOP SPEED). All the dyeing parameters remained constant for both samples.

Fabric (I): 2% DR243, (II): 4 g cotton fabric, (III): 15 g L⁻¹ salt (NaCl), bath report: 1/50.

Samples (A) and (B) were compared by measuring their visible spectrophotometry (color coordinates) using the CIELab system in DATACOLOR 600TM, where L^* indicates lightness, and a^* and b^* are the chromaticity coordinates. To calculate the total deviation (dE^*), the Kubelkae Munk equation [Eq. (5)] was used [17]. C^* is the Chroma, and h is the hue angle.

$$\Delta E^* = \sqrt{(\Delta L^*)^2 + (\Delta a^*)^2 + (\Delta b^*)^2} \tag{12}$$

where dE^* is the total deviation, dL^* is the lightness axis deviation, da^* is the green–red axis deviation, and db^* is the yellow–blue axis deviation.

2.10. Recycling water processing

The water resulting from the dye bath is photocatalyzed by 0.6 g L⁻¹ of ZnO for 240 min, with solar irradiation. The photocatalytic treatment was repeated five times, for the second, third, fourth, and fifth treatment, a bath was prepared with the same preparation conditions of the first solution (DE): dye (dye concentration DR243: 50 ppm, 15 g L⁻¹ salt (NaCl)). The concentration of NaCl was measured by the conductivity meter using the method described earlier in Rosa’s article in Rosa et al. [17]. Fig. 2 describes the process of recycling water.

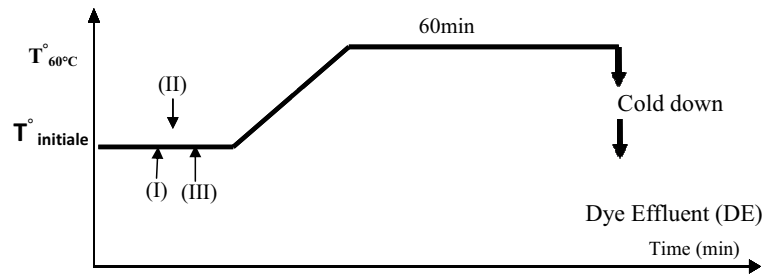


Fig. 1. Dyeing sequence with DR 243.

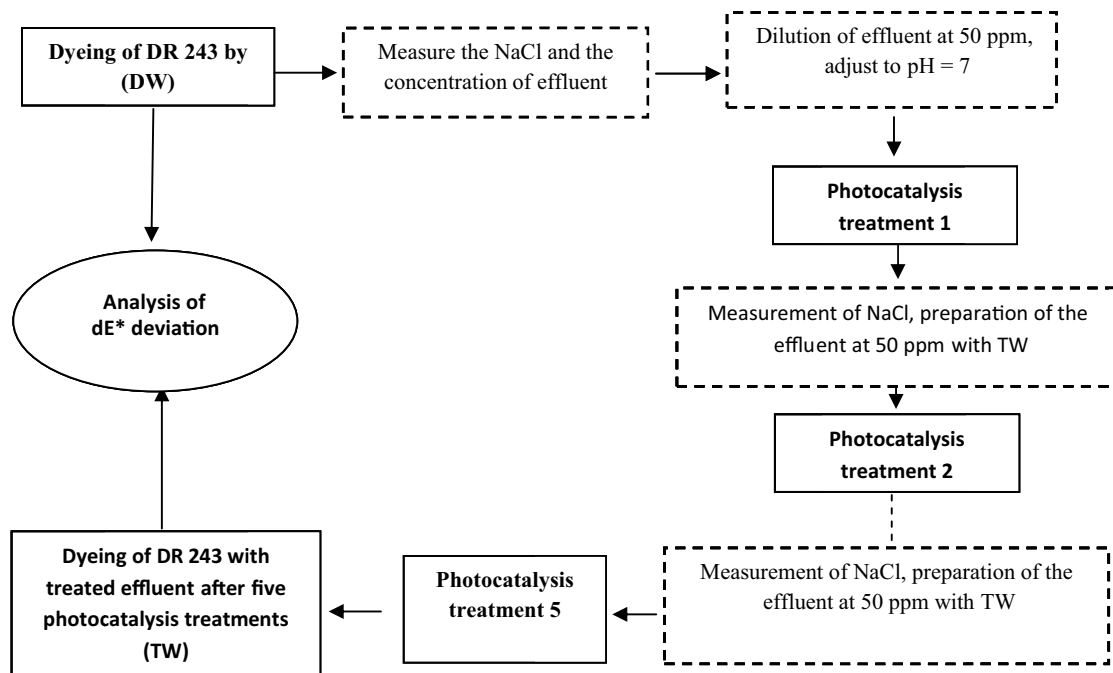


Fig. 2. Processes of water recycling.

3. Results and discussions

3.1. Characterization

3.1.1. SEM analysis

Electron microscopy examination was used to investigate the structural and morphological features of the prepared samples. From Fig. 3a, we can see that the particles have a spherical shape and are uniformly distributed. Larger particles in this Fig. 3 may be aggregates of the smaller particles.

3.1.2. XRD analysis

The XRD of ZnO reveals the properties through the XRD pattern shown in Fig. 3b. In this Fig. 3, 10 peaks are located at 31.75° , 34.44° , 36.25° , 47.54° , 56.55° , 62.87° , 66.38° , 67.91° , 69.05° , and 72.61° , and they have been keenly indexed as hexagonal phase (wurtzite). These values correspond to the file (JCPDS Card No. 00-005-0664). The average particle size of the sample has been calculated using the Williamson–Hall (W–H) method; it was found to be 52.12 nm.

3.1.3. FT-IR analysis

Fig. 3c shows the FT-IR spectra of the synthesized ZnO particles. The peaks at 599 cm^{-1} are related to the stretching vibrations of Zn–O bonds. The peak at $3,436\text{ cm}^{-1}$ indicates the presence of –OH residue [18,19], and the $1,000\text{--}2,000\text{ cm}^{-1}$ bending indicates the presence of hydroxyl residue which is due to atmospheric moisture [20].

3.1.4. UV-visible absorption spectrum

The ZnO specter (Fig. 3d) shows a single broad and intense absorbance band of about 400 nm, which confirmed the ZnO formation. This band is due to the charge transfer of the valence band (mainly formed by the 2p orbitals of the oxide anions) to the conduction band (mainly formed by the 3d orbitals of Zn^{2+} cations) [21]. We can also detect some absorption above 400 nm; this can be attributed to the development of shallow levels inside the band gap due to the presence of foreign atoms in the lattice. The shift of the absorption peak to a higher wavelength indicates the decrease of the optical band gap (first bright exciton energy) [22].

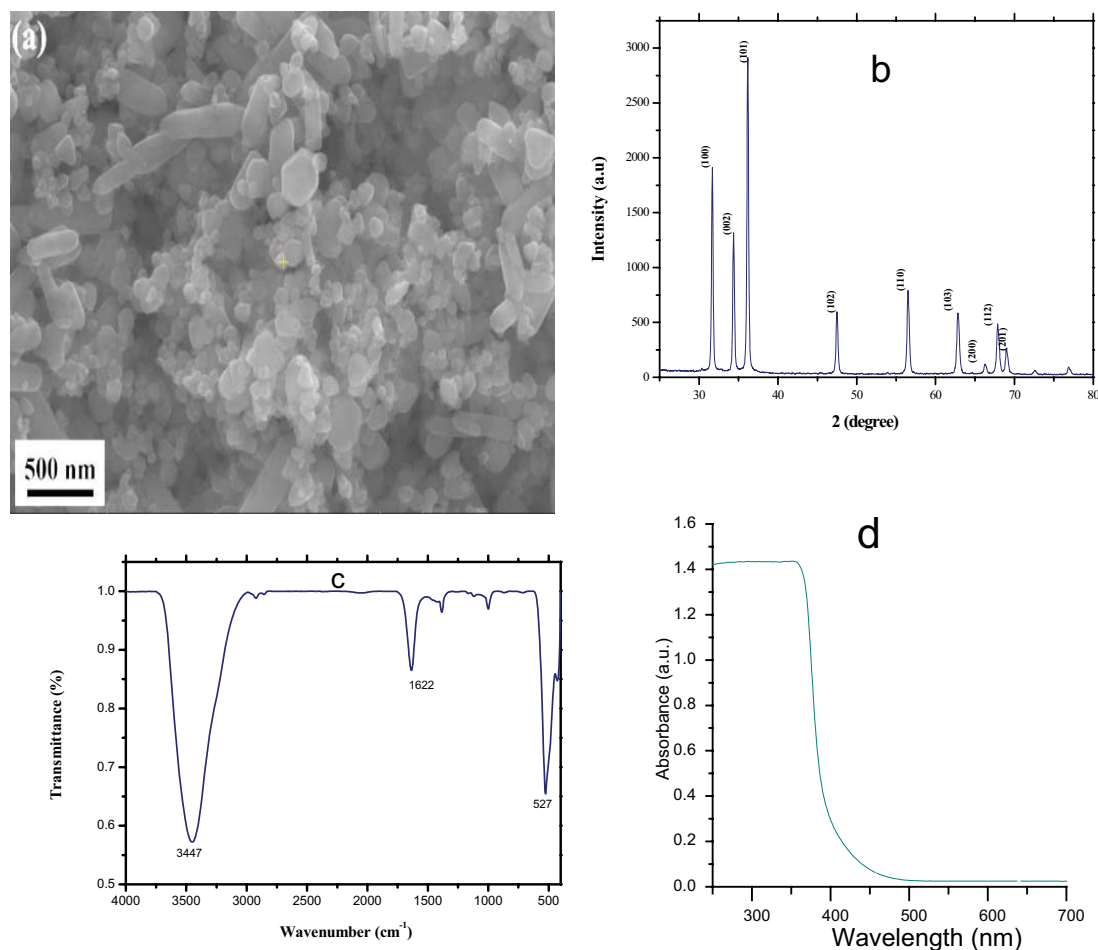


Fig. 3. (a) SEM, (b) XRD, (c) FT-IR, and (d) UV-vis of ZnO nanoparticles.

3.2. Dye degradation

3.2.1. UV-VIS/HPLC analysis

Degradation experiments of DY86 (diazoique dye), DR243 (diazoique dye), and DB71 (triazoiqye dye) were conducted with UV-VIS and with HPLC at 30, 60, 120, 180, and 240 min. In all test runs, the other operational parameters were kept constant; an initial experiment with UV light alone (photolysis) did not cause any significant changes in the degradation of this dye, however, it caused about 30% of the dye concentration reduction with ZnO alone without UV light (adsorption).

As shown in Figs. 4a and b, the value of the residual concentration (C_t/C_0) of decolorization and degradation of the three dyes decreased with the increase of irradiation time during 0–30 and 60 min, because during this period, more quantity of the dyes is adsorbed by the catalyst surface and consequently, more quantity of dyes was degraded due to the generation of an increased amount of hydroxyl radicals by the catalyst. After 60 min, the residual concentration of decolorization and degradation of the three dyes slow down; this was probably due to the competition between the parent molecules and the intermediate products formed during degradation [23,24].

We found also that DR243 and DB71 have a better photocatalytic decolorization and degradation than DY86.

All parameters of dye degradation were the same; therefore, we have been able to explain the difference and the order of degradation, by the molecular structure and substituents of the dyes. In our case, the degradation efficiency of the diazoique dye DR243 is almost the same as the one of the triazoiqye dye DB71, and much better than that of the diazoique dye DY86.

These observations suggest that degradation does not depend on the azo groups but on other structural groups.

The parameters of the reaction kinetic models for the degradation of DY86, DR243, and DB71, and the results of zero-, first-, second-order, and BMG kinetic models are given in Table 2.

Comparing the correlation coefficients (R^2) obtained from Table 2, it can be observed that the fitting of the zero-, first-, and second-order models to the experimental data is not high for all dyes: DY86, DR243, and DB71 due to the low correlation coefficients. However, the results of R^2 for BMG kinetic (0.94: DY86, 0.97: DR243, and 0.99: DB71) are much better than the other kinetics; therefore the BMG kinetic is the best model to describe the discoloration of (DY86, DR243, and DB71). The physical meaning of $1/m$ was the initial dye

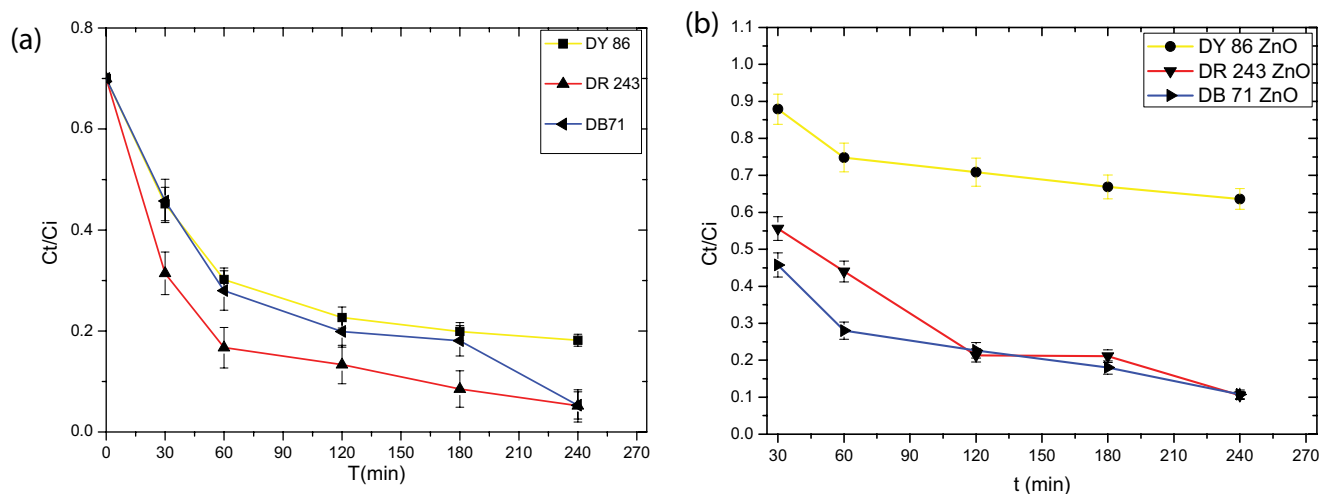


Fig. 4. (a) Dyes discoloration and (b) dyes degradation.

Table 2
Kinetics study of DY86, DR243, and DB71

Dye	Zero-order		First-order		Second-order		BMG		
	k_0 ($\mu\text{mol L}^{-1} \text{min}^{-1}$)	R^2	k_1 (min^{-1})	R^2	k_2 ($\text{L } \mu\text{mol}^{-1}$)	R^2	$1/m$ (min^{-1})	$1/b$	R^2
DY86	0.068	0.81	0.0017	0.85	4.45E-05	0.89	0.011	0.4	0.94
DR243	0.156	0.77	0.008	0.94	0.0007	0.91	0.04	0.93	0.97
DB71	0.141	0.63	0.008	0.87	0.0006	0.94	0.069	0.9	0.99

discoloration rate in the process. The higher $1/m$ value indicated the faster initial discoloration rate of dye. When t was long and approaching infinity, the $1/b$ value represents the maximum theoretical dye degradation fraction, which was equal to the maximum degradation capacity of the photocatalytic process after a very long or infinite reaction time, which was equal to the maximum degradation process [25].

From Table 2, we observed that the $1/m$ value of DB71 is 0.069, DR243 is 0.04, and DY86 is 0.011 (min^{-1}); which means that DB71 is the first dye which was degraded, followed by DR243, and finally DY86 was the last degraded one.

3.2.2. HPLC analysis

To improve the formation of intermediate products, we analyze the HPLC dyes' diagram at 0 min and 240 min, at $t = 0$ we have the chromatogram of untreated dyes: DY86, DR243, and DB71. A major peak was obtained at a retention time of RT: 2.63 min for DY86, RT: 2.51 min for DR243, and RT: 3.96 min for DB71. After 240 min of treatment, the peak surface area was reduced for all the three dyes confirming their degradation, and a new peak with new retention times was clearly shown in the case of DY86 (Fig. 5), confirming the parent dye's transformation into intermediate products for this dye.

3.2.3. LC/MS/MS studies

The (LC/MS/MS) analysis was carried out at 240 min in order to gain a further understanding of the difference in

the degradation of this trichromatic dye, and the products formed during the degradation process.

3.2.3.1. Direct Yellow DY86

The LC/MS/MS analysis of degraded DY86, showed four major peaks at $m/z = 680.9$, 352, 278, and 106 (Table 3; Fig. 6). A degradation path is proposed in Fig. 7 based on these m/z values. The path is proposed to start with the OH radicals' attack which destroys the chromophoric system through azo bond cleavage, and leads to the formation of possible intermediates with $m/z = 680.9$ corresponding to $[\text{C}_{29}\text{H}_{29}\text{N}_9\text{O}_7\text{S}_2]$, and $m/z = 278$ corresponding to $[\text{C}_{10}\text{H}_9\text{N}_2\text{NaO}_4\text{S}]$. The deamination and desulfonation of a peak at $m/z = 680.9$ $[\text{C}_{29}\text{H}_{29}\text{N}_9\text{O}_7\text{S}_2]$ may produce another peak at $m/z = 352$ corresponding to $[\text{C}_{19}\text{H}_{22}\text{N}_6\text{O}]$. The peak at $m/z = 106$ $[\text{C}_6\text{H}_7\text{NO}]$ is formed by desulfonation of a peak at $m/z = 278$, and the peak at $m/z = 88$ $[\text{C}_6\text{H}_6\text{O}]$ was attributed to the deamination of $m/z = 106$. A complete degradation of the $[\text{C}_{10}\text{H}_9\text{N}_2\text{NaO}_4\text{S}]$: $m/z = 278$ dye is pronounced by the formation of CO_2 and H_2O ; the peaks at $m/z = 680.9$ and 352 correspond probably to $[\text{C}_{29}\text{H}_{29}\text{N}_9\text{O}_7\text{S}_2]$ and $[\text{C}_{19}\text{H}_{22}\text{N}_6\text{O}]$: (((4,6-bis(p-tolylamino)-1,3,5-triazin-2-yl)methyl)amino) methanol with two methyl groups, make the DY86 resistant to degradation.

We complete the degradation of DY86 at the same conditions: a concentration of (50 ppm) at solar irradiation, and the presence of (0.6 g L^{-1}) ZnO during 360 min, the residual concentration of degradation remains constant. We conclude

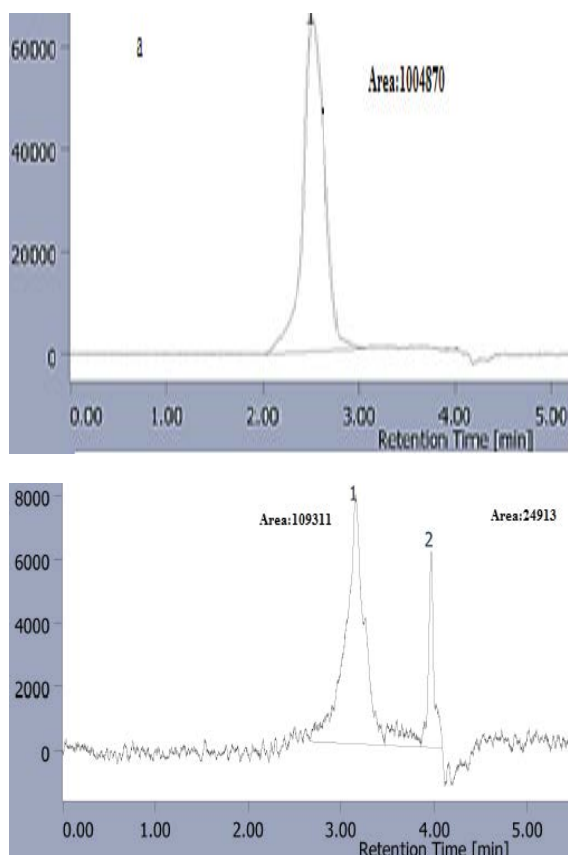


Fig. 5. HPLC: chromatograms analysis: (a) DY86 at 0 min and (b) DY86 at 240 min.

that at these conditions, DY86 is resistant to degradation, maybe due to the dyes' specific molecular structure, or to the presence of alkyl-CH₃ group in DY86's molecular structure, which can decrease its degradation. This ascertainment was confirmed earlier by Khataee and Kasiri [26], or we need more contact time of degradation because the kinetic of degradation of DY86 is lower compared to DB71 and DR243.

3.2.3.2. Direct Red DR243

The LC/MS/MS analysis of degraded DR243, showed three major peaks at $m/z = 279$, 157, and 106 (Table 4, Fig. 8), no peaks are shown between 600 and 1,200 m/z . The degradation path of DR243, as shown in Fig. 9, is proposed with the attack of OH radicals, which cleaved the azo

Table 4
LC/MS/MS data (m/z) of the identified uncommon degraded products of DR243

m/z	Chemical formula	Proposed structure name
279	C ₁₀ H ₉ N ₂ NaO ₄ S	Sodium 3,7-diamino-4-hydroxynaphthalene-2-sulfonate
157	C ₅ H ₉ N ₅ O	Not be generated
	C ₁₀ H ₉ NO	2-aminonaphthalen-1-ol
106	C ₆ H ₇ NO	2-aminopheno
	C ₇ H ₈ O	Anisole

bond N–N, the C–N bond, and also the desulfonation in dye molecule, and formed five intermediate products with a peak at $m/z = 279$ [C₁₀H₉N₂NaO₄S], $m/z = 157$ [C₅H₉N₅O], [C₁₀H₉NO], and $m/z = 106$ [C₆H₇NO], [C₇H₈O].

3.2.3.3. Direct Blue 71

The LC/MS/MS data of the identified degraded products are provided in (Table 5, Fig. 10); the degradation path is proposed in Fig. 11. The attack of OH radical cleaved two of the azo bonds N=N, and led to the formation of species with $m/z = 391$ corresponding to [C₂₀H₁₆N₄O₃S], $m/z = 346$ corresponding to [C₁₀H₇NNa₂O₆S₂], and $m/z = 279$ corresponding to [C₁₀H₉N₂NaO₄S]. The desulfonation and subsequent oxidation of $m/z = 279$ and 346 led to the formation of peaks corresponding to $m/z = 106$ (2-aminophenol), and the chromophoric system's destruction through the azo bond. The desulfonation and subsequent oxidation of $m/z = 391$ led to the formation of possible intermediates: benzene-1 and 4-diamine, with $m/z = 106$. A further attack leads to the complete mineralization of the dye through phenol and aniline, and therefore leads to its mineralization.

A comparison of LC/MS/MS for this combination of trichromatic dyes (DY86), (DR243), and (DB71) revealed major intermediate species formed during the degradation process. The proposed pathway can be regarded as a sign of successful dye degradation of (DR243) and (DB71), and a confirmation of an incomplete degradation of (DY86).

3.3 Effect of pH

To investigate the effect of pH on the decolorization efficiency of DY86, DR243, and DB71, experiments were

Table 3
LC/MS/MS data (m/z) of the identified uncommon degraded products of DY86

m/z	Chemical formula	Proposed structure name
680.9	C ₂₉ H ₂₉ N ₉ O ₇ S ₂	3-((5-((4-((3-amino-4-methylphenyl)amino)-6-(hydroxymethyl)amino)methyl)-1,3,5-triazin-2-yl)amino)-2-methylphenyl)diazenyl)naphthalene-1,5-diyl bis(hydrogen sulfite)
352	C ₁₉ H ₂₂ N ₆ O	(((4,6-bis(p-tolylamino)-1,3,5-triazin-2-yl)methyl)amino)methanol
278.2	C ₁₀ H ₉ N ₂ NaO ₄ S	Sodium 7-hydrazinyl-5-hydroxynaphthalen-1-yl sulfite
106.3	C ₆ H ₇ NO	2-aminophenol

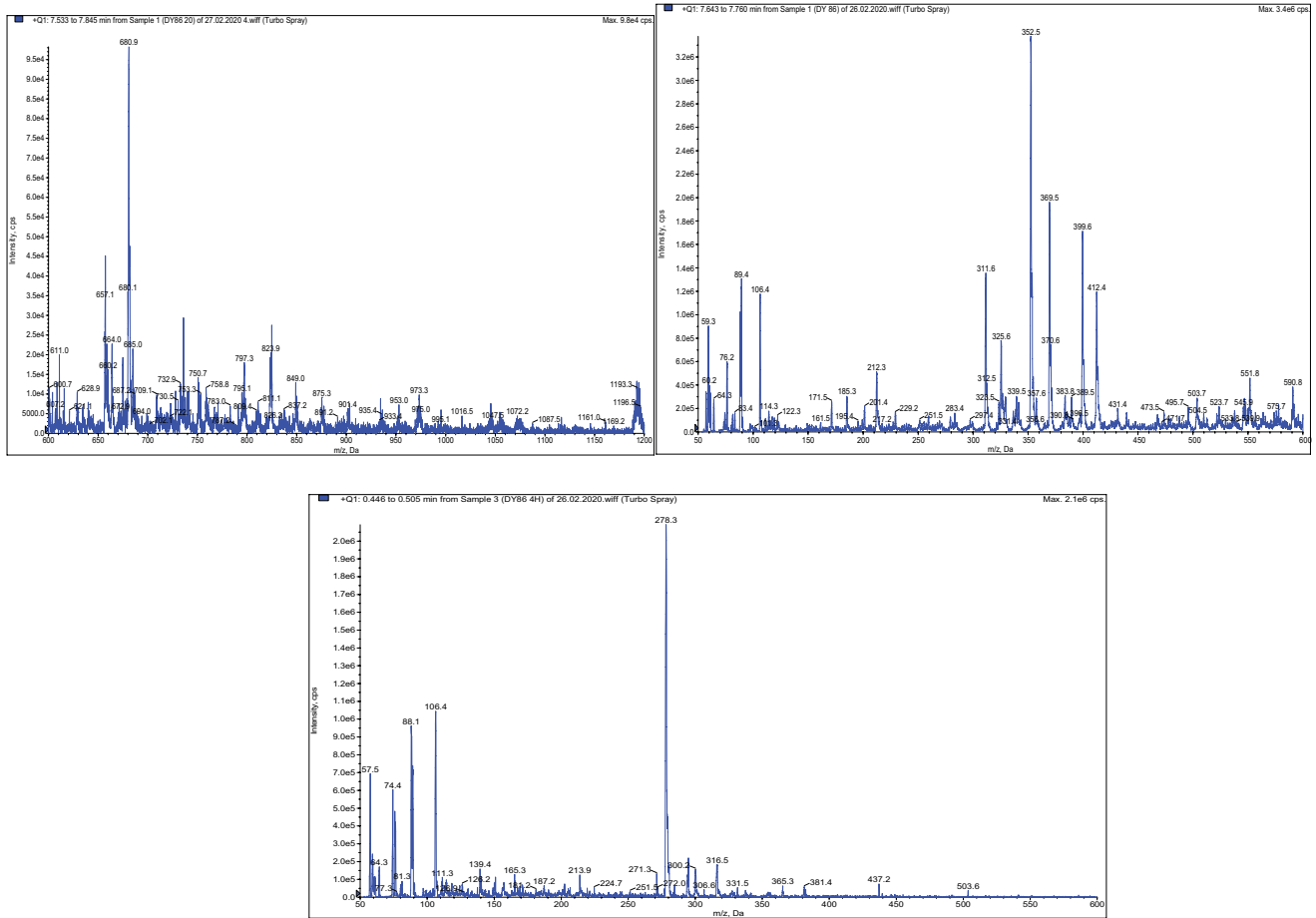


Fig. 6. LC/MS/MS spectra of DY86 in the mass range m/z 0–1,200.

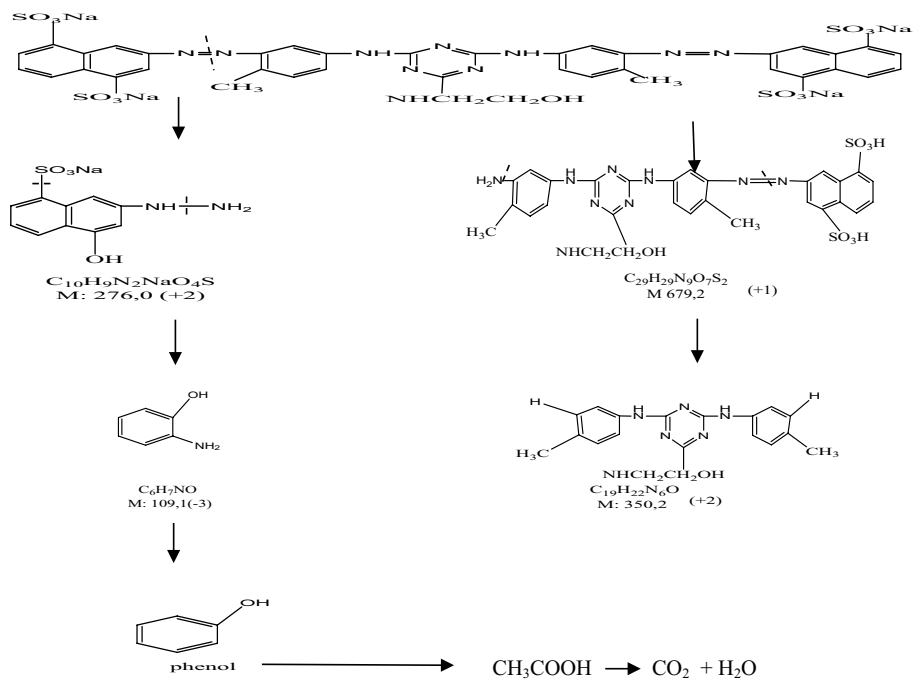


Fig. 7. Degradation pathway of DY86.

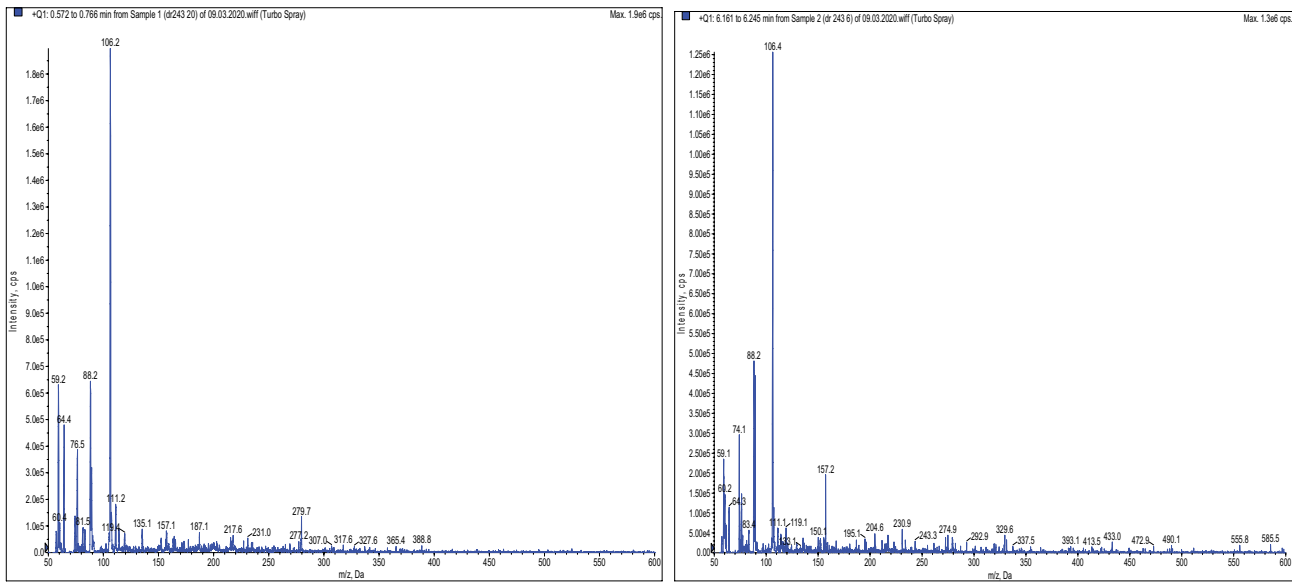


Fig. 8. LC/MS/MS spectra of DR243 in the mass range m/z 0–600.

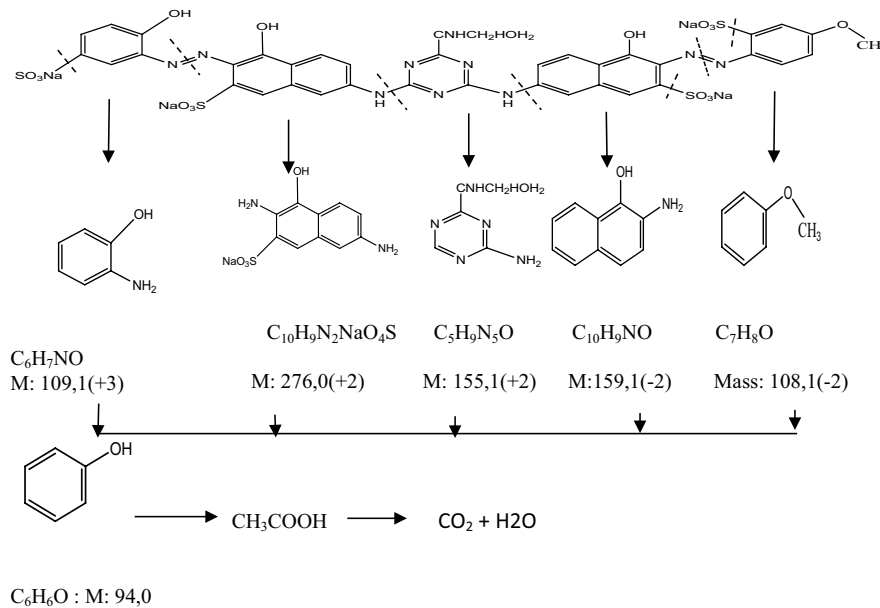


Fig. 9. Degradation pathway of DR243.

carried out at various pH values: 3.0, pH_7 , and 11, at a constant dye concentration of 50 mg L^{-1} , and a catalyst loading of 0.6 g L^{-1} (ZnO). The decolorization efficiency of the three dyes at different pH values is shown in Fig. 12.

At $pH = 3$ and 11, there is a decrease in the residual concentration; this happens because at low pH, the electrostatic interactions between the positive surface of the catalyst and the coloring anions, cause strong adsorption of the latter on the metal oxide support, and at alkaline pH, the presence of a large amount of OH ions increases significantly the photocatalyst degradation of the dye [27]. This explains that dyes at both alkaline and acid pH are better discolored than at pH_7 .

3.4. Effect of anions

The existence of inorganic anions such as chloride Cl^- and sulfate SO_4^{2-} is considerably common in direct dye wastewaters; for this reason, the effects of the presence of these anions in direct dye effluent are evaluated. A mixture of ZnO (0.6 g L^{-1}) and DR243 (50 ppm) was irradiated in the presence of sodium chloride 15 g L^{-1} (experience 1), and in the presence of sodium sulfate 15 g L^{-1} (experience 2).

The results show that the efficiency of the % decolorization decreases from 98% to 57% in the presence of Cl^- and from 98% to 61% in the presence of SO_4^{2-} . Therefore, the

Table 5
LC/MS/MS data (m/z) of the identified uncommon degraded products of DB71

m/z	Chemical formula	Proposed structure name
391	$C_{10}H_7NNa_2O_6S_2$	Could not be generated
346.6	$C_{10}H_7NNa_2O_6S_2$	Sodium 3-aminonaphthalene-1,5-disulfonate
279	$C_{10}H_9N_2NaO_4S$	Sodium 3,7-diamino-4-hydroxynaphthalene-1-sulfonate
106	C_6H_7NO	2-aminophenol
	$C_6H_8N_2$	Benzene-1,4-diamine

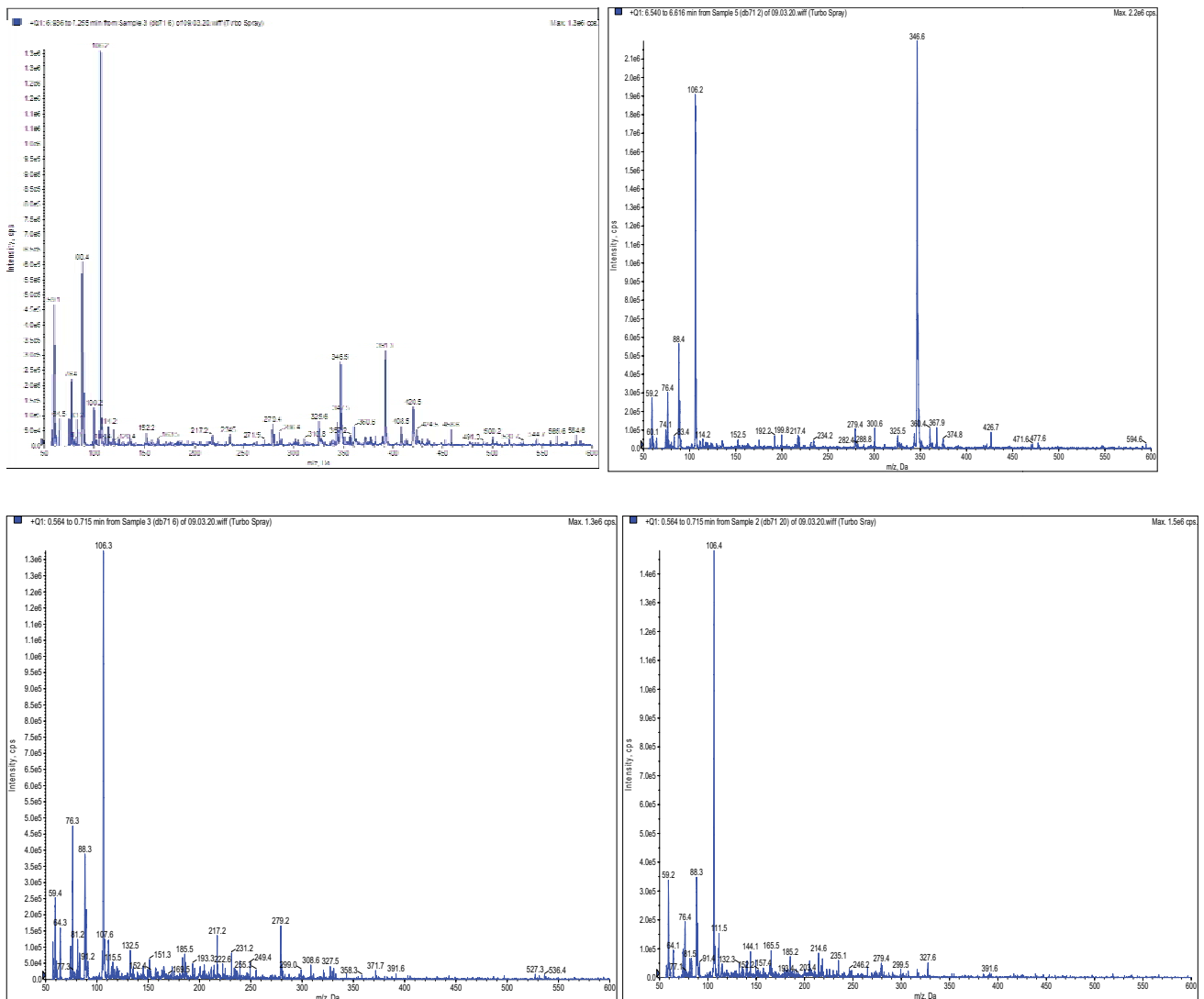


Fig. 10. LC/MS/MS spectra of DB71 in the mass range m/z 0–600.

anions have a negative effect on the decolorization of the direct dye. This effect can be explained by:

The presence of chloride is due to its hole and hydroxyl radical scavenging effect, which occurs as follows [28]:



Similarly, the presence of sulfate ions can react with the positive holes (h^+) and hydroxyl radical (OH^\bullet) in solution because $SO_4^{\bullet-}$ is less reactive than OH^\bullet and h_{VB}^+ , therefore, the presence of sulfate ions can react with the positive holes

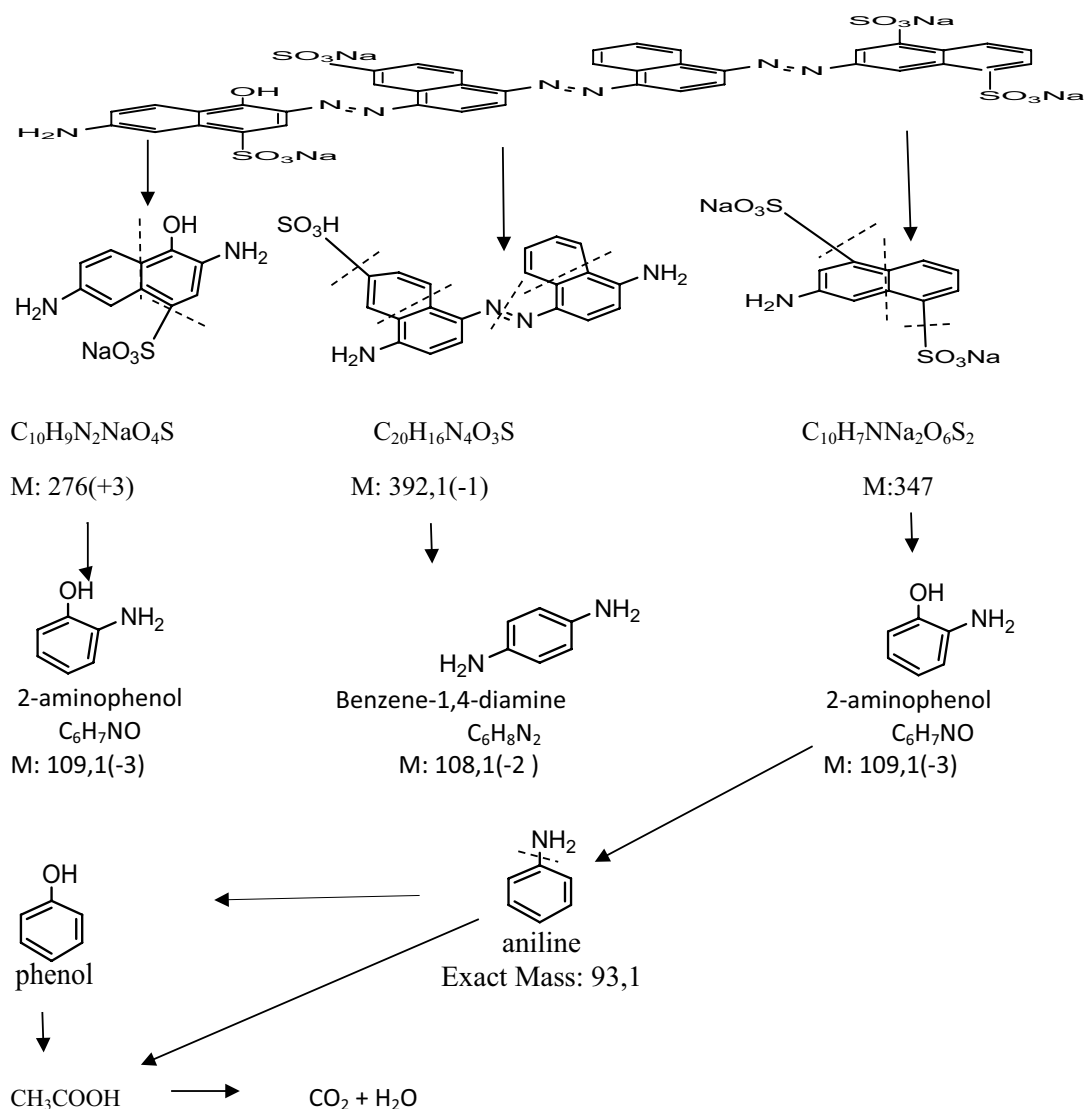


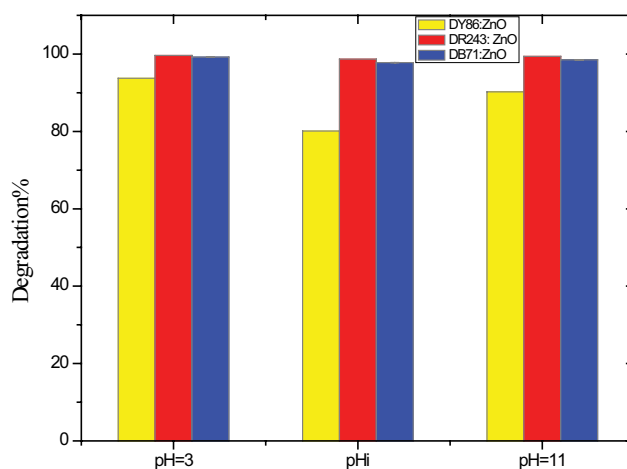
Fig. 11. Degradation pathway of DB71.

($h_{\nu_B}^+$) and hydroxyl radical (OH), and hinder the photocatalytic degradation of dyes as follows:



3.5. Mineralization studies COD

COD gives a measure of the dye's degradation and generates intermediates during the irradiation, and also a measure of the organic's oxygen equivalent. Table 6 gives the rate of COD at $t = 30, 60, 120, 180,$ and 240 min, which was calculated relative to the initial COD value at $t = 0$. As represented, the $R\%$ COD values increases with an increase in irradiation time. The $R\%$ COD increased from 9.6% to 47.3% for DY86, from 22.22% to 88.7% for DR243, and from 18.33% to 87.5% for DB71; these results confirm that the degradation of the three dyes depends

Fig. 12. Effect of pH on photocatalytic decolorization ($C_0 = 50 \text{ mg L}^{-1}$; $ZnO = 0.6 \text{ g L}^{-1}$; $T = 30^\circ\text{C}$).

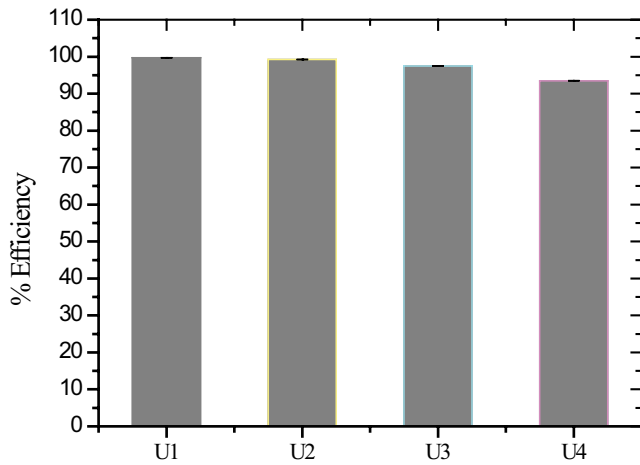


Fig. 13. Reuse of the photocatalyst.

Table 6
COD values vs. irradiation time: (amount of ZnO (0.6 g L⁻¹), dye concentration 50 ppm) under solar irradiation

		Time: min				
		30	60	120	180	240
R % COD	DY86	9.59	28.66	31.51	45.2	47.3
	DR243	22.22	50.00	55.56	66.67	88.7
	DB71	18.33	44.67	50.00	58.33	87.5

Table 7
COD values after the first and the last treatments

	% Decolourization	% Degradation	R % COD
First treatment	95%	91%	86%
Last treatment	94%	85%	80%

on the time of photocatalysis and the percentage of degradation.

3.6. Reuse of the photocatalyst

We observe from Fig. 13 below that the catalyst is stable and could be used three times with 93% efficiency. This small decrease in the activity can be due to the loss of mass catalyst during the washing and centrifugation process [29]. Similar results were observed by Sahoo et al. [30], and Barkul et al. [31].

The loss of catalyst during the washing and centrifugation procedure is verified by the gravimetric analysis. A solution was prepared following the same procedure as the nanoparticles' regeneration: the nanoparticles' mass was 30 mg in the dry state, their volume was 50 mL, and the washing and centrifugation were at 5,000 tr min⁻¹, and finally weighing the nanoparticles and determining their mass by difference. This operation was repeated three times with the same protocol. We observed that we

lose about 4.5%–5.4% every cycle; these results prove that the loss of photocatalytic activity is due to the nanoparticles' mass loss during the washing and centrifugation operations.

3.7. Recycling water treatment

3.7.1. Chemical oxygen demand

The COD after the first and the last treatment of wastewater, and the percentage of degradation and decolorization after the photocatalytic treatment were observed before, to find whether it was fit for reuse or further recycling in the dyeing process (Table 7).

From Table 7, we observe a stabilization in the decolorization and a decrease in degradation %. The COD percentages did not affect the dyeing quality (the total deviation, *dE*) of fabric, because they were negligible at that time [32].

The decrease in R% COD and degradation % could be due to the evaporation of water after five photocatalytic treatments; the decolorization value (94%) helped to obtain an acceptable *dE* [17].

3.7.2. Color difference

The color difference between fabric (A) dyed with (DW) and fabric (B) dyed reusing water obtained from effluent after complete decolorization of color by photocatalysis treatment (TW) was analyzed; the deviations' values between (A) and (B) found for the dyed fabric samples, are shown in Table 8.

It was seen that the total deviation (*dE*) is very small and did not exceed 1, which is an acceptable value for the textile industry. From this result, we can conclude that the water made by photocatalytic treatment can be reused in the dyeing process. The reason of this experience is to recycling and to economize the water used in the dyeing industry.

4. Conclusion

This study evaluated the photodegradation of three direct dyes (DY86, DR243, and DB71) with synthesized ZnO. The characterization results (SEM, XRD, UV-vis, and FT-IR) confirmed the ZnO nanostructures. The experimental results indicate that the structure of dyes, pH, and anions affect photocatalysis treatment.

The indications obtained from both HPLC and LC/MS/MS confirmed the degradation of dyes into intermediate

Table 8
Deviation colors between (A) and (B)

Bath	Results
<i>da</i> *	-0.09
<i>db</i> *	0.33
<i>dL</i> *	-0.13
<i>dC</i> *	-0.02
<i>dH</i> *	0.21
<i>dE</i> *	0.25

products, and many of them led to even complete mineralization for DR243 and DB71, and a partial one for DY86.

The nanoparticles' recycling revealed that they lost a little of their photocatalytic activity, during the washing and centrifugation processes.

The water, treated five times by the photocatalytic process, was recycled to dye the fabric samples, and the results showed that this water could be reused and had a similar color as compared to the fresh one.

References

- [1] X. Zeng, J. Yang, L. Shi, L. Li, M. Gao, Synthesis of multi-shelled ZnO hollow microspheres and their improved photocatalytic activity, *Nanoscale Res. Lett.*, 9 (2014) 468, doi: 10.1186/1556-276X-9-468.
- [2] A. Khanna, V.K. Shetty, Solar light induced photocatalytic degradation of Reactive Blue 220 (RB-220) dye with highly efficient Ag@TiO₂ core-shell nanoparticles: a comparison with UV photocatalysis, *Solar Energy*, 99 (2014) 67–76.
- [3] A. El Nemr, M.A. Hassaan, F.F. Madkour, HPLC-MS/MS mechanistic study of Direct Yellow 12 dye degradation using ultraviolet assisted ozone process, *J. Water Environ. Nanotechnol.*, 3 (2018) 1–11.
- [4] A.F. Shojaei, A. Shams-Nateri, M. Ghomashpasand, Comparative study of photocatalytic activities of magnetically separable WO₃/TiO₂/Fe₃O₄ nanocomposites and TiO₂, WO₃/TiO₂ and TiO₂/Fe₃O₄ under visible light irradiation, *Superlattices Microstruct.*, 88 (2015) 211–224.
- [5] S.K. Kansal, N. Kaur, S. Singh, Photocatalytic degradation of two commercial reactive dyes in aqueous phase using nanophotocatalysts, *Nanoscale Res. Lett.*, 4 (2009) 709–716, doi: 10.1007/s11671-009-9300-3.
- [6] S.K. Sharma, H. Bhunia, P.K. Bajpai, Photocatalytic decolorization kinetics and adsorption isotherms of a mixture of two anionic azo dyes: Reactive Red 120 and Reactive Black 5, *Desal. Water Treat.*, 44 (2012) 261–268.
- [7] S. Boumaza, F. Kaouah, D. Hamane, M. Trari, S. Omeiri, Z. Bendjama, Visible light assisted decolorization of azo dyes: Direct Red 16 and Direct Blue 71 in aqueous solution on the p-CuFeO₂/n-ZnO system, *J. Mol. Catal. A: Chem.*, 393 (2014) 156–165.
- [8] T. Chen, Y. Zheng, J.-M. Lin, G. Chen, Study on the photocatalytic degradation of methyl orange in water using Ag/ZnO as catalyst by liquid chromatography electrospray ionization ion-trap mass spectrometry, *J. Am. Soc. Mass Spectrom.*, 19 (2008) 997–1003.
- [9] S. Hisaindee, M. Meetani, M. Rauf, Application of LC-MS to the analysis of advanced oxidation process (AOP) degradation of dye products and reaction mechanisms, *TrAC, Trends Anal. Chem.*, 49 (2013) 31–44.
- [10] P. Bansal, D. Singh, D. Sud, Photocatalytic degradation of azo dye in aqueous TiO₂ suspension: reaction pathway and identification of intermediates products by LC/MS, *Sep. Purif. Technol.*, 72 (2010) 357–365.
- [11] M. Meetani, S. Hisaindee, F. Abdullah, S. Ashraf, M. Rauf, Liquid chromatography tandem mass spectrometry analysis of photodegradation of a diazo compound: a mechanistic study, *Chemosphere*, 80 (2010) 422–427.
- [12] Y. Ding, C. Sun, X. Xu, Simultaneous identification of nine carcinogenic dyes from textiles by liquid chromatography/electrospray ionization mass spectrometry via negative/positive ion switching mode, *Eur. J. Mass Spectrom.*, 15 (2009) 705–713.
- [13] B. Viswanathan, Photocatalytic degradation of dyes: an overview, *Curr. Catal.*, 7 (2018) 99–121.
- [14] B. Savi, L. Rodrigues, E. Uggioni, A. Bernardin, OBTENÇÃO DE NANOPARTÍCULAS DE ZnO A PARTIR DE PROCESSAMENTO SOL-GEL, 55° Congresso Brasileiro de Cerâmica, Porto de Galinhas, PE, Brasil, 2011.
- [15] A.S. Yargic, N. Ozbay, Fenton and photo-Fenton degradation of reaktoset Brilliant Orange/P-2R and telon turquoise/M-GGL dyes: effect of operating parameters and kinetic study, *Int. J. Adv. Res. Chem. Sci.*, 3 (2016) 38–45.
- [16] C. Sidney Santana, M.D. Nicodemos Ramos, C.C. Vieira Velloso, A. Aguiar, Kinetic evaluation of dye decolorization by Fenton processes in the presence of 3-hydroxyanthranilic acid, *Int. J. Environ. Res. Public Health*, 16 (2019) 1602, doi: 10.3390/ijerph16091602.
- [17] J.M. Rosa, A.M. Fileti, E.B. Tambourgi, J.C. Santana, Dyeing of cotton with reactive dyestuffs: the continuous reuse of textile wastewater effluent treated by ultraviolet/hydrogen peroxide homogeneous photocatalysis, *J. Clean. Prod.*, 90 (2015) 60–65.
- [18] K. Nejati, Z. Rezvani, R. Pakizevand, Synthesis of ZnO nanoparticles and investigation of the ionic template effect on their size and shape, *Int. Nano Lett.*, 1 (2011) 75–81.
- [19] D. Djouadi, M. Meddouri, A. Chelouche, Structural and optical characterizations of ZnO aerogel nanopowder synthesized from zinc acetate ethanolic solution, *Opt. Mater.*, 37 (2014) 567–571.
- [20] G. Nagaraju, S. Prashanth, M. Shastri, K. Yathish, C. Anupama, D. Rangappa, Electrochemical heavy metal detection, photocatalytic, photoluminescence, biodiesel production and antibacterial activities of Ag–ZnO nanomaterial, *Mater. Res. Bull.*, 94 (2017) 54–63.
- [21] A. Miri, N. Mahdinejad, O. Ebrahimi, M. Khatami, M. Sarani, Zinc oxide nanoparticles: biosynthesis, characterization, antifungal and cytotoxic activity, *Mater. Sci. Eng., C*, 104 (2019) 109981, doi: 10.1016/j.msec.2019.109981.
- [22] M. Pudukudy, Z. Yaakob, Facile synthesis of quasi spherical ZnO nanoparticles with excellent photocatalytic activity, *J. Cluster Sci.*, 26 (2015) 1187–1201.
- [23] M. Al-Amin, S.C. Dey, T.U. Rashid, M. Ashaduzzaman, S.M. Shamsuddin, Solar assisted photocatalytic degradation of reactive azo dyes in presence of anatase titanium dioxide, *Int. J. Latest Res. Eng. Technol.*, 2 (2016) 14–21.
- [24] R. Rajeswari, S. Kanmani, A study on degradation of pesticide wastewater by TiO₂ photocatalysis, *J. Sci. Ind. Res.*, 68 (2009) 1063–1067.
- [25] H.-Y. Xu, T.-N. Shi, L.-C. Wu, S.-Y. Qi, Discoloration of methyl orange in the presence of schorl and H₂O₂: kinetics and mechanism, *Water Air Soil Pollut.*, 224 (2013) 1740, doi: 10.1007/s11270-013-1740-9.
- [26] A. Khataee, M.B. Kasiri, Photocatalytic degradation of organic dyes in the presence of nanostructured titanium dioxide: influence of the chemical structure of dyes, *J. Mol. Catal. A: Chem.*, 328 (2010) 8–26.
- [27] B. Neppolian, H. Choi, S. Sakthivel, B. Arabindoo, V. Murugesan, Solar/UV-induced photocatalytic degradation of three commercial textile dyes, *J. Hazard. Mater.*, 89 (2002) 303–317.
- [28] M. Rauf, S.S. Ashraf, Fundamental principles and application of heterogeneous photocatalytic degradation of dyes in solution, *Chem. Eng. J.*, 151 (2009) 10–18.
- [29] J. Kaur, M. Sharma, O. Pandey, Synthesis, characterization, photocatalytic and reusability studies of capped ZnS nanoparticles, *Bull. Mater. Sci.*, 37 (2014) 931–940.
- [30] C. Sahoo, A. Gupta, A. Pal, Photocatalytic degradation of Methyl Red dye in aqueous solutions under UV irradiation using Ag⁺ doped TiO₂, *Desalination*, 181 (2005) 91–100.
- [31] R.P. Barkul, M.K. Patil, S.M. Patil, V.B. Shevale, S.D. Delekar, Sunlight-assisted photocatalytic degradation of textile effluent and Rhodamine B by using iodine doped TiO₂ nanoparticles, *J. Photochem. Photobiol., A*, 349 (2017) 138–147.
- [32] A. Ali, I.A. Shaikh, T. Abid, F. Samina, S. Islam, A. Khalid, N. Firdous, M.T. Javed, Reuse of textile wastewater after treating with combined process of chemical coagulation and electrocoagulation, *Text. Ind.*, 4 (2019) 2565–2570.